Carbohydrate Polymers 99 (2014) 249–256

Contents lists available at ScienceDirect

Carbohydrate Polymers

journal homepage: www.elsevier.com/locate/carbpol

Ionically gelled alginate foams: Physical properties controlled by type, amount and source of gelling ions

Therese Andersen[a,b,*], Jan Egil Melvik[a], Olav Gåserød[a], Eben Alsberg[c,d,e], Bjørn E. Christensen[b]

[a] FMC BioPolymer AS/NovaMatrix, Sandvika, Norway
[b] Department of Biotechnology, NOBIPOL, Norwegian University of Science and Technology, Trondheim, Norway
[c] Department of Biomedical Engineering, Case Western Reserve University, Cleveland, OH, USA
[d] Department of Orthopaedic Surgery, Case Western Reserve University, Cleveland, OH, USA
[e] National Center for Regenerative Medicine in the Devision of General Medical Sciences, Case Western Reserve University, Cleveland, OH, USA

ARTICLE INFO

Article history:
Received 30 June 2013
Received in revised form 12 August 2013
Accepted 15 August 2013
Available online 23 August 2013

Keywords:
Biomaterial
Polysaccharide
Porous
Hydrogel
Gelation
Gelation kinetics

ABSTRACT

A new and flexible method for preparation of dry macroporous alginate foams with the capability of absorbing physiological solutions has been developed, which may find use within areas such as wound healing, cell culture, drug delivery and tissue engineering. The present study demonstrates how the gelation rate of the alginate and degree of ionic crosslinking can be utilized to control the physical foam properties. The rate of released Ca^{2+}/Sr^{2+} gelling ions available for interaction with the alginate was influenced by the concentration and physical characteristics of $CaCO_3$/$SrCO_3$ particles. The method of preparation of such foams allows, as described herein, tailoring of the pore structure, hydration properties and mechanical integrity in a manner not possible by other techniques.

1. Introduction

Three-dimensional scaffolds for pharmaceutical and biomedical applications can be prepared from both natural and synthetic materials by different techniques (Grayson, Martens, Eng, Radisic, & Vunjak-Novakovic, 2009; Lee & Mooney, 2012). The polysaccharide alginate has been found particularly useful within these areas (Augst, Kong, & Mooney, 2006; Drury & Mooney, 2003; Jain, Ayen, Domb, & Kumar, 2011; Tønnesen & Karlsen, 2002). Alginates are naturally occurring anionic linear (unbranched) polysaccharides, which can be extracted from kelp, brown seaweed, and some bacteria. Alginates are salts of alginic acid and consist of residues of (1 → 4) linked β-D-mannuronate (M) and its C-5-epimer α-L-guluronate (G), with a source specific distribution of residues organized in either G-blocks (...GGGG...), alternating blocks (...MGMGMG...) or M-blocks (...MMMM...) (Andersen, Melvik, Gåserød, Alsberg, & Christensen, 2012; Andersen, Strand, Formo, Alsberg, & Christensen, 2012). The G-blocks are the key structural elements giving rise to gelation with divalent cations such as Ca^{2+} and Sr^{2+} ions through partial chain dimerization.(Andersen, Melvik, et al., 2012; Andersen, Strand, et al., 2012b; Draget, Smidsrød, & Skjåk-Bræk, 2005) Tuning of the properties of alginate based hydrogels is therefore possible and will depend on the monomer composition of the alginate, its molecular weight, gelling ions and concentrations. As alginates form hydrogels under gentle gelling conditions, the gel structure may be used to entrap cells, and cell-hydrogel interactions may be enabled by the use of alginates with known concentrations of conjugated cell signaling molecules such as peptides (Rowley, Madlambayan, & Mooney, 1999) or sulphate (Sapir, Kryukov, & Cohen, 2011). Hydrogels may also support new tissue formation and function as an extracellular matrix (ECM), with non-immunogenic and adjustable rigidity and bioresorption properties (Alsberg et al., 2003; Huebsch et al., 2010; Kong, Alsberg, Kaigler, Lee, & Mooney, 2004; Lee & Mooney, 2012; Place, Rojo, Gentleman, Sardinha, & Stevens, 2011; Simmons, Alsberg, Hsiong, Kim, & Mooney, 2004).

Alginate molecules in alginate scaffolds may, when in contact with physiologic solutions *in vivo*, leak out of the scaffold at the implantation site as gelling ions are exchanged by non-gelling sodium ions. Thus, the bioresorption properties can be tuned as are they are strongly influenced by the amount and type of gelling ions initially bound to the alginate, type of alginate and the alginate molecular weight (Alsberg et al., 2003; Boontheekul, Kong, &

* Corresponding author at: FMC BioPolymer AS/NovaMatrix, Industriveien 33, 1337 Sandvika, Norway. Tel.: +47 69 815 513; fax: +47 69 815 510.
E-mail address: therese.andersen@fmc.com (T. Andersen).

0144-8617/$ – see front matter © 2013 Elsevier Ltd. All rights reserved.
http://dx.doi.org/10.1016/j.carbpol.2013.08.036

Mooney, 2005; Kong et al., 2004; Kong, Smith, & Mooney, 2003; Lee & Mooney, 2012; Place et al., 2011; Simmons et al., 2004). Mammals do not have the capability to enzymatically degrade alginate molecules. However, a slow cleavage of the glycosidic bonds will take place, and the rate constant can be estimated to about $3 \times 10^{-6}\,h^{-1}$ (Kristiansen, Tomren, & Christensen, 2011). Renal clearance may be allowed for alginates below approximately 50 kDa (Al-Shamkhani & Duncan, 1995).

Macroporous scaffolds as foams or sponges have recently been recognized as implantable materials providing improved cell invasion and improved mass transport of nutrients, oxygen and waste removal compared to non-porous hydrogels (Hwang et al., 2010; Shapiro & Cohen, 1997). Several studies have demonstrated benefits utilizing this format for tissue engineering and regenerative medicine applications (Dvir-Ginzberg, Elkayam, & Cohen, 2008; Li, Ramay, Hauch, Xiao, & Zhang, 2005; Miralles et al., 2001; Re'em, Tsur-Gang, & Cohen, 2010; Sapir et al., 2011). Porous alginate scaffolds have also been evaluated as carriers of therapeutically active ingredients (Freeman, Kedem, & Cohen, 2008; Lai, Abu'Khalil, & Craig, 2003), and the format may be advantageous as the surface area is considerably increased, which may accelerate the release of actives and scaffold degradation. A recent publication highlights the ability to compress macroporous alginate hydrogels without permanent deformation or mechanical destruction, demonstrating their potential for minimally invasive delivery of cells and therapeutic agents (Bencherif et al., 2012). The selection of amount and type of gelling ions and alginate is important tools to control the release of incorporated materials by diffusion or disintegration of the scaffold itself (Hegge et al., 2011; Hegge, Andersen, Melvik, Kristensen, & Tønnesen, 2010; Holte, Tønnesen, & Karlsen, 2006; Kuo & Ma, 2001a; Lee & Mooney, 2012; Place et al., 2011; Wee & Gombotz, 1998). Although, calcium is the gelling ion that is most commonly used for preparation of alginate hydrogels, strontium may be an alternative for some applications and has shown benefit over calcium for bone tissue engineering where the release of strontium ions upregulated the phenotype marker genes of osteoblasts cultured within such gels (Place et al., 2011). Additionally, dry porous alginate scaffolds have the ability to absorb high amounts of wound exudates and form conditions beneficial for wound healing (Boateng, Matthews, Stevens, & Eccleston, 2008). Lyophilization combined with different freezing regimes (Thornton, Alsberg, Albertelli, & Mooney, 2004; Zmora, Glicklis, & Cohen, 2002) is currently the main technique for preparation of alginate foams (Barbetta, Barigelli, & Dentini, 2009; Leone et al., 2004; Li et al., 2005; Miralles et al., 2001; Shapiro & Cohen, 1997; Thornton et al., 2004; Zmora et al., 2002). A recent review summarizes techniques of cryogelation in general for preparation of biomaterials for biomedical applications (Henderson, Ladewig, Haylock, McLean, & O'Connor, 2013).

Recently we published a new method for preparation of air dried alginate foams (Andersen, Melvik, et al., 2012; Andersen, Strand, et al., 2012b). The method is based on internal gelation of the alginate (Draget, Østgaard & Smidsrød, 1991; Draget et al., 2005; Kuo & Ma, 2001b) and enables a uniform distribution of molecules. Thus, a known concentration of gelling ions throughout the alginate foam is achieved. The study showed how operational parameters as well as alginate macromolecular properties were utilized to tailor physical foam characteristics.

The present work describes how the gelling reaction, *i.e.* the time dependent interaction between alginate molecules and gelling ions that takes place before drying of the alginate foams, can be tuned to vary the physical characteristics of the dried foams. It is known that the gelling reaction depends upon the release rate of gelling ions from $CaCO_3$ (Moe, Draget, Skjåk-Bræk, & Smidsrød, 1995). However, this knowledge has not previously been utilized to control the characteristics of macroporous alginate foams. Herein, different approaches for tuning of this reaction are evaluated including gelling time after foam preparation before drying, specific surface area of $CaCO_3$ particles, concentration of $CaCO_3$ and the use of $SrCO_3$ as an alternative source for gelling ions. The dried foams were characterized with respect to pore structure, average pore size, liquid absorbency properties and mechanical properties.

2. Experimental

2.1. Alginate foam preparation

Alginate foams were prepared and characterized as described previously with few modifications (Andersen, Melvik, et al., 2012; Andersen, Strand, et al., 2012b). In brief, a dispersion of calcium carbonate ($CaCO_3$, HuberCal Elite 850, 500, 250 and 150, J.M. Huber Corp., Quincy, IL) or strontium carbonate ($SrCO_3$, 99.9+ %, Sigma–Aldrich, Steinheim, Germany) was first sonicated for 2×15 s in water to disrupt agglomerations (40 Hz, Branson 200) (the dispersion of $SrCO_3$ was further dispersed using an Ultra-Turrax T25 (8000 rpm) from IKA Werke). Next, a premade aqueous alginate solution (stock solution) of 4.1 wt%, final concentration of 2.0 wt%, PRONOVA UP MVG (F_G: 0.69, M_W: 207,000 g/mol, water content: 9 wt%, NovaMatrix, FMC BioPolymer, Sandvika, Norway) and the other components presented in Table A1 in Supporting Data were mixed and air was incorporated using a Hobart N50 mixer. The alginate was saturated with different levels of calcium (Ca^{2+}) and strontium (Sr^{2+}) ions, assuming 100% saturation equals 1 mol divalent cation per 2 mol alginate monomers. The molar ratio between Ca^{2+}/Sr^{2+} and glucono-δ-lactone (GDL, Lysactone T, Roquette, Lestrem, France) was kept constant at 0.5. The wet foam had a density of 21–23 g/100 mL and was transferred to 4 mm high trays. Subsequent gelling for 1 h and drying in a forced air drying oven at 80 °C for 75 min gave large pliable sheets of foam.

2.2. Characteristic of $CaCO_3$ and $SrCO_3$ particles

The median particle size of $CaCO_3$ and $SrCO_3$ were determined using a particle size analyzer, Mastersizer S, from Malvern Instruments. The particles were dispersed in isopropanol (refractive index: 1.39) and treated with ultrasound for 3×15 s to disrupt agglomerations. The average value ± standard error (SE) from the median values of 9 runs from 3 separate sample additions is reported. Refractive index/imaginary indexes of $CaCO_3$ and $SrCO_3$ were 1.590/0.010 and 1.518/0.010, respectively. The reported specific particle surface areas were provided by the supplier.

2.3. Gelling kinetics with different types and amounts of $CaCO_3/SrCO_3$

Detailed formulations for the study of gelling kinetics using different saturations of gelling ions are presented in Table A2. Compositions and weights of the stock solutions are presented in Table A3. The concentrations of alginate, $CaCO_3/SrCO_3$ and GDL are the same as in the foam formulations, but HPMC, plasticizers and air was not included. The alginate concentration was kept constant at 2.0 wt%, whereas the saturation of gelling ions was varied from 17% to 84% with a constant molar ratio between Ca^{2+}/Sr^{2+} and GDL of 0.5. 84% saturation with Ca^{2+} was used when the influence of $CaCO_3$ particle size was evaluated. An aqueous dispersion containing alginate and $SrCO_3/CaCO_3$ was prepared by first dispersing the carbonate in MQ-H_2O and sonicating for 3×10 s. The alginate powder was added to the dispersion and a stock solution of alginate and $SrCO_3/CaCO_3$ was prepared using Ultra-Turrax T25. A weighing boat was used to weigh and mix the suspension of alginate/carbonate and a freshly made solution of GDL. 2.5–3.0 mL of the suspension was applied to a Bohlin 120 CVO rheometer

(Malvern, software version 6.50.5.7). The gelling kinetics of the different formulations was followed by oscillatory measurements at 1 Hz frequency and 0.001 strain with a 1.000 mm gap and serrated plates (PP40) at 20 °C. The plates were covered with a lid to prevent drying of the gel. The measurements started 2 min after the GDL was first mixed with the alginate/carbonate suspension. The time required to reach the solution/gelation (sol/gel) transition point was registered. The sol/gel transition point occurs when loss modulus (G'') = storage modulus (G') and the phase angle (δ) = 45°.

2.4. Pore characterization

Test methods for characterization of pore structure and pore size distribution on the upper part of the dry foam was determined by light microscopy images as described previously (Andersen, Melvik, et al., 2012; Andersen, Strand, et al., 2012b). In brief, images obtained by Leica DM 2500 microscope with the attached camera Leica DFC420 were used to manually draw 50 lines of pore diameters on three images for each foam (software: Leica application suite 2.4.0 R1) and the average value of the 150 lines was calculated. Also, the level of transparency by hydrating the dried foams in MQ-H_2O was evaluated qualitatively related to the interconnectivity of the pore network.

2.5. Absorbency capacity

The method for this absorbency test is based on BS EN 13726-1:2002 (BSI British Standards, 2002) and calculations of absorbency and drainage were accomplished as described previously (Andersen, Melvik, et al., 2012; Andersen, Strand, et al., 2012b). In brief, pieces of 5 × 5 cm dry foam were conditioned in a closed container containing a saturated solution of sodium nitrite (Merck, Darmstadt, Germany) overnight to obtain a constant moisture content. The container has a humidity of 66% at 20 °C. The dry foam weight of the conditioned foam pieces was recorded (W_1) before they were immersed in 40 times their weight of a model physiological solution (Solution A) at 37 °C comprising 2.5 mM Ca^{2+} ($CaCl_2 \times 2H_2O$; Sigma–Aldrich, Riedel-de Haën, Seelze, Germany) and 142 mM Na^+ (NaCl; Merck, Darmstadt, Germany). After 30 min at 37 °C the foam was lifted in one corner with forceps and allowed to passively drip for 30 s (W_3) before the weight of the foam was recorded (W_2). Absorbency capacity and fluid drainage were calculated by the following equations and reported as the average of 6 parallels ± SE:

$$\text{Absorbency capacity (g/g)} = \frac{W_2 - W_1}{W_1}$$

$$\text{Fluid drainage (\%)} = \frac{W_3}{W_3 + (W_2 - W_1)} \times 100$$

2.6. Mechanical properties of rehydrated foam

Mechanical properties of rehydrated alginate foams described by Young's modulus, tensile strength and nominal strain at break, were characterized as described previously (Andersen, Melvik, et al., 2012; Andersen, Strand, et al., 2012b). In brief, a texture analyzer TA-XTplus with tensile grips (A/TG) and software TEE 32 (v. 4090) from Stable Micro Systems, were used to characterize foams that were cut according to test specimen Type I described in ASTM test method D638-10 (ASTM International, 2010), and rehydrated in Hanks' balanced salt solution (H8264; Sigma–Aldrich, Steinheim, Germany). Excess solution was removed on three layers of one ply hand tissue paper and fixed to the tensile grips. Tensile stress was applied at a constant strain rate of 0.50 mm/s until foam rupture.

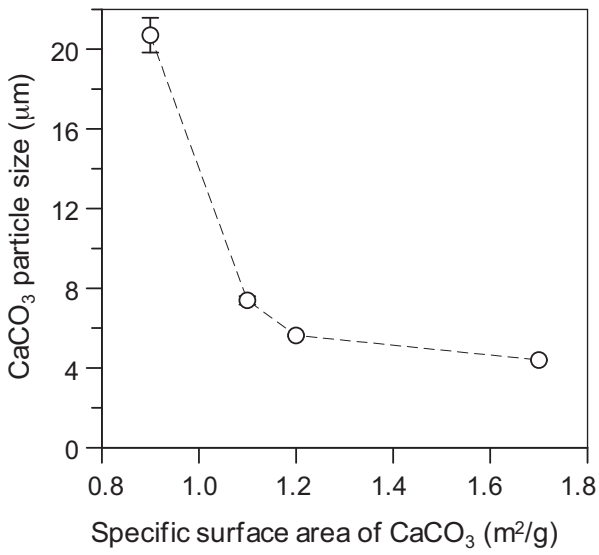

Fig. 1. Size and specific surface area of the different $CaCO_3$ particles. Error bars depict SE when exceeding the size of the symbols.

2.7. Statistical analysis

Statistical analysis was carried out using single factor ANOVA. All variables are expressed as mean ± SE.

3. Results and discussion

3.1. Influence of carbonate particle types and concentration on alginate gelling kinetics

Different $CaCO_3$ and $SrCO_3$ particles were tested in order to evaluate the influence on alginate gelling kinetics. The suspensions tested did not contain HPMC, plasticizers or air, but these ingredients are not expected to influence on the gelling kinetics and release of gelling ions from the carbonate salts. The four types of $CaCO_3$ particles used in this study differed in size and specific surface area (Fig. 1). The particle size of the $SrCO_3$ used was (0.5 ± 0.01 µm, specific surface area not available), hence smaller than all types of $CaCO_3$ particles tested.

The particle shape may vary among different carbonate grades and will highly influence the particle size. This effect is taken into consideration when using the specific surface area. The release rate of Ca^{2+} will also relate to the specific surface area of the particles, and the specific surface area is therefore referred to from here.

As expected, the $CaCO_3$ specific surface area increases by decreasing particle size. Hence, the dissolution rate of carbonate and release of Ca^{2+} will be more rapid as the specific surface area increases. The rate of gel formation is for internal gelling dependent on the free Ca^{2+} ions available at each time. This was controlled by varying the specific surface area of $CaCO_3$ particles and amount $CaCO_3$ added (calcium saturation).

The gelation of alginate hydrogels (alginate, GDL and $CaCO_3/SrCO_3$) was monitored by oscillatory rheometry. The time to reach sol/gel transition for formulations with different $CaCO_3$ particles while the saturation was kept constant at 84% saturation is presented in Fig. 2A. Fig. 2B shows the time to reach sol/gel transition with different saturations of calcium while the same type of $CaCO_3$ particles (1.2 m^2/g) and a constant ratio of $CaCO_3$/GDL. G' was within the range of 22–23 Pa and 21–25 Pa at the sol/gel transition points for the measurements in Fig. 2A and B, respectively. The gelling kinetics of an alginate hydrogel made from $SrCO_3$ at 84% saturation was also evaluated. The particles with

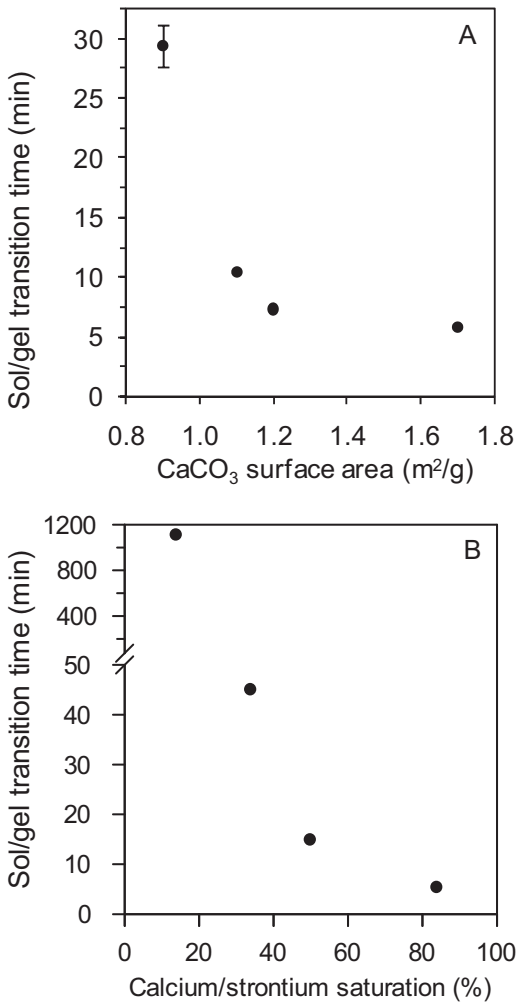

Fig. 2. Time to reach sol/gel transition as a function of specific surface area of $CaCO_3$ at a calcium saturation of 84% (A) and calcium saturation with $CaCO_3$ particles with a specific surface area of 1.2 m^2/g (B). $n = 3$ and error bars depict SE when exceeding the size of the symbols.

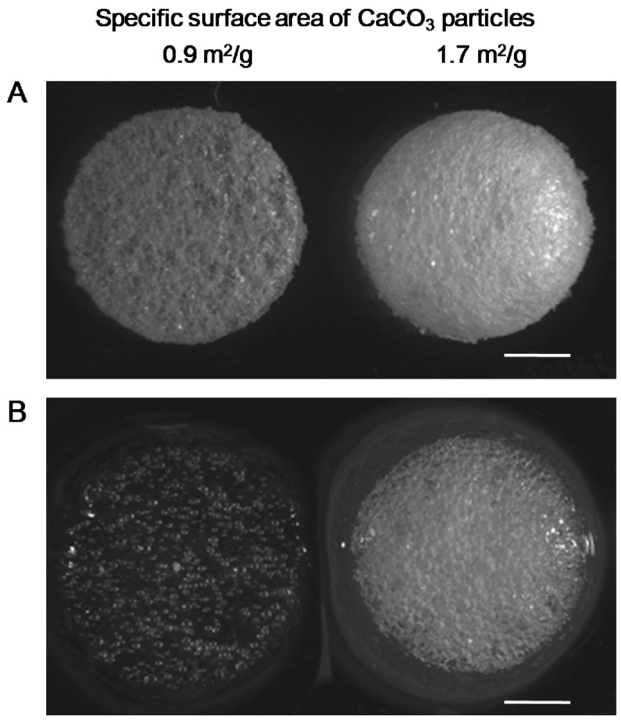

Fig. 3. Foams made with $CaCO_3$ particles of different specific surface area before (A) and after (B) hydration in MQ-water. Scale bar: 250 mm.

strontium were smaller than the calcium particles and showed the shortest sol/gel transition time of 3.01 ± 0.10 min and a G' of 25 ± 2 Pa. The fast gelation rate with strontium ions was likely due to the smaller particles in addition to the higher affinity of alginate for strontium ions compared to calcium ions (Haug & Smidsrød, 1970).

Clearly, the gelation rate increased by increasing particle specific surface area (Fig. 2A) and increasing calcium saturation (Fig. 2B). Similar data presenting the influence on the gelation rate by the size of $CaCO_3$ particles has been previously shown by Moe et al. (1995).

More than 18 h were required to reach the sol/gel transition point for the gel with 17% calcium saturation (Fig. 2B) which may indicate that this saturation level is just exceeding what is needed to achieve sol/gel transition. The exact mechanisms and concentration of calcium needed to form an alginate hydrogel are not known, but the so-called "egg-box" model is widely accepted and describes chain-chain associations being induced by the presence of calcium forming junction zones between chains of G-blocks and/or MG-blocks that present cavities suitable to accommodate divalent cations in a chelate type of binding (Donati et al., 2005). The Ca^{2+} interaction with alginate has been described as an auto-cooperative process, where consecutive G-residues (G-blocks) are filled first and thereby forming egg-box dimers followed by gel formation (Draget et al., 2005). Fang et al. (2007) suggested that Ca^{2+} binding to alginate is a sequential three step process controlled by the ratio between Ca^{2+} and G-monomers. Ratios below 0.25 are involved in the step of mono-complexation, followed by formation of egg-box dimers at ratios between 0.25 and 0.55, and for higher ratios formation inter-cluster or intra-cluster associated multimers. A calcium saturation of 17% equals a Ca^{2+}/G molar ratio of 0.12, which according to Fang et al. (2007) is below the level required for formation of dimers and thus hydrogel formation.

The data presented for 17% saturation in Fig. 2B may, however, indicate that the alginate and calcium ions over time form gel structures. The alginate concentration may explain the different results, as the proposed mechanism was demonstrated for an alginate concentration four times below what is used in the present study (Fang et al., 2007). The critical concentration of Ca^{2+} required to induce alginate gelation is likely dependent on alginate concentration and alginate type.

3.2. Foam structure

The influence of the gelling kinetics varied by type of $CaCO_3$ particle on foam structure was investigated by visual evaluation. Micrographs of two dry foam discs (Fig. 3A) and the same two discs rehydrated in MQ-water (Fig. 3B) made with different $CaCO_3$ particles (smallest and largest specific surface areas) illustrated substantial variations in pore size and transparency. The foam made from the $CaCO_3$ particles with the smallest specific surface area contained visually larger pores and became more transparent when rehydrated. The difference in transparency may be attributed to an increased interconnectivity of the pores as a larger portion of the foam is filled with liquid. Low interconnectivity can be related to them amount closed pores and the visually less transparent foam as the pores are occupied by entrapped air.

The influence of the gelling kinetics on the average pore size was investigated for foams made from the different $CaCO_3$ particles (Fig. 1), $SrCO_3$ particles and different calcium saturations. Within

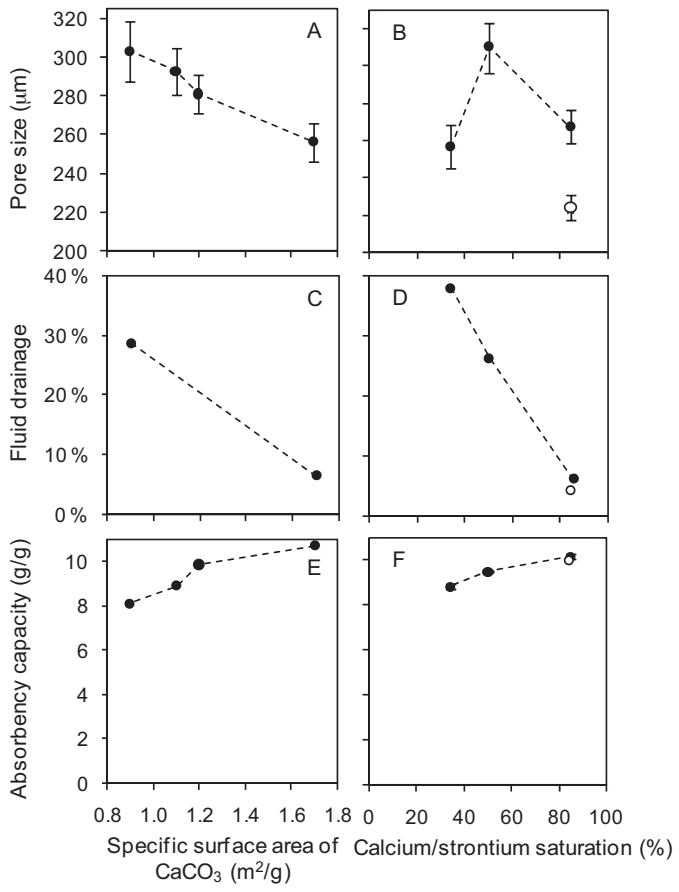

Fig. 4. The average foam pore size, fluid drainage and absorbency capacity evaluated for foams made from $CaCO_3$ of different specific surface area at constant calcium saturation of 84% (A, C and E), different calcium saturations with the same type of $CaCO_3$ with a specific surface area of 1.2 m^2/g and from $SrCO_3$ at 84% saturation (B, D and F). Dotted lines are added as guides to the eye. $n = 50$ pores × 3 foam samples (A and B), $n = 6$ (C–F) and error bars depict SE when exceeding size of the symbols. Symbols: (●) $CaCO_3$, (○) $SrCO_3$.

the range of $CaCO_3$ particles tested, the pore size of the foams decreased with increasing specific surface areas (Fig. 4A). The pore sizes of the foams with different calcium saturations were similar for the lowest and highest saturations, whereas the foam with intermediate saturation had somewhat larger pores ($p < 0.01$; Fig. 4B). The smallest pores were found for the foam saturated with 84% strontium (Fig. 4B). The change in pore sizes is attributed to various degrees of coalescence of air bubbles prior to gelation or drying. Slower gelling and increased coalescence contribute to larger pores and also higher pore interconnectivity in the dried foam as the pore walls probably are more likely to break during the gelling step.

Although the average pore size was similar for the foams with the highest and lowest calcium saturation, the pore size distribution was somewhat more uniform for the foams saturated with 84% compared to the foams with 34% saturation, where 80% of the pores were within the range of 149–422 μm and 101–488 μm for the 84% saturated and 34% saturated, respectively. The small pores for the foam from $SrCO_3$ were expected due to its small particle size and fast gelling kinetics.

3.3. Fluid drainage

When a dry alginate foam was immersed in a model physiological solution, the pores of the foam were filled with this solution and the pore walls were rehydrated by swelling. Fluid drainage measures the ability of the foam to retain the absorbed solution and refers to the immediate and passive loss of fluid within 30 s after retrieving the fully hydrated foam from the liquid bath. For 84% saturated foams with small specific surface area $CaCO_3$, and consequently large pores, extensive drainage (29%) took place whereas foams with small pores retained most of the fluid (6%) (Fig. 4C). The extent of drainage also decreased with increasing calcium saturation (same type of $CaCO_3$ particles) (Fig. 4D). The fluid drainage of 84% saturated foams was similar for forms gelled with calcium and strontium. The high drainage of fluid from foams with lower calcium saturation and lower specific surface area of $CaCO_3$ is likely due to a more interconnected pore network as formed during the low gelation rates (Figs. 2 and 3).

3.4. Absorbency

The absorbency capacity (absorbed and retained fluid after draining) was found to slightly increase with increasing $CaCO_3$ specific surface area for 84% saturated foams (Fig. 4E) and with increasing calcium saturation ($CaCO_3$ particles of 1.2 m^2/g) (Fig. 4F). The absorbency of 84% saturated foams was similar for forms gelled with calcium and strontium. The foam structure will influence the absorbency rate of liquids as the foams with a highly interconnected pore network more easily will be filled and the amount of visible entrapped air bubbles are lower (Fig. 3). In addition to the liquid the remains in the pores of the foam by capillary forces, the foam absorbency capacity involves the amount of liquid in the rehydrated pore walls which is influenced by the type of molecular associations formed between alginate and calcium. Such associations will be influenced by the concentration of Ca^{2+} bound to alginate (Funami et al., 2009) and may further affect the ability to rehydrate and absorb liquid. The main mechanism that controls the amount of liquid that is retained in the foams made with different $CaCO_3$ particles is likely solely the pore structure. For the foams made with different amounts of gelling ions, also the amount of liquid in the pore walls contributes to the determined capacities. Rehydration or swelling, of alginate structures with lower concentrations of gelling ions is expected to be higher due to a more flexible network of alginate molecules. The results in Fig. 4D and F indicate this as the fluid drainage (due to change in pore structure) is reduced dramatically at increasing saturations, while the absorbency capacity just slightly increases.

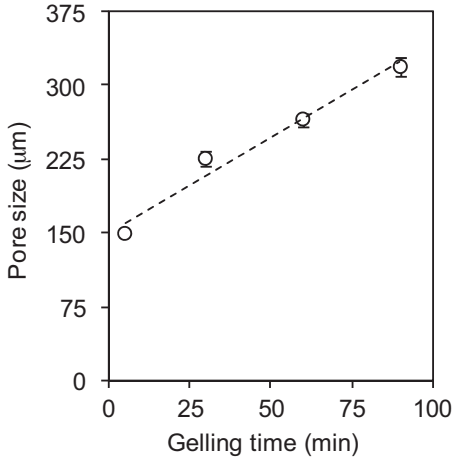

Fig. 5. Average foam pore size of dried foams as a function of gelling time before drying for foams made from $CaCO_3$ particles with a specific surface area of 1.2 m^2/g and 84% calcium saturation. $n = 50$ pores × 3 foam samples and error bars depict SE when exceeding the symbols. The straight line was fitted by the method of least squares ($R^2 = 0.97$).

3.5. Gelling time before drying

Coalescence of air bubbles in the wet foam has been shown to be influenced by the gelling kinetics, but also drying of the wet foam will prevent coalescence. The influence of gelling time before the foam was placed in the oven on average pore size was investigated for a foam made from $CaCO_3$ particles with a specific surface area of 1.2 m^2/g and calcium added to saturate the alginate by 84%. A linear increase in average pore size from about 150 μm to 300 μm was observed when the gelling time increased from 5 min to 90 min (Fig. 5). This trend however, is not expected to continue indefinitely for longer gelling times as the foam at some time point will be gelled sufficiently to stop further coalescence.

3.6. Mechanical properties of rehydrated foams

To examine whether the mechanical properties of foams were influenced by gelling time, specific surface area of $CaCO_3$ and calcium/strontium saturation, the mechanical properties of the same set of foams as shown in Figs. 4 and 5 were determined (Fig. 6). No dimensional changes of the foams were seen by hydration in Hanks' solution, except for the foam made with 34% calcium saturation that showed about 15% in increase in length and width. In this case the tensile measurements and calculations were adjusted accordingly.

Fig. 6A–C presents the mechanical properties of foams prepared with different gelling times and a constant specific surface area of $CaCO_3$ particles of 1.2 m^2/g and calcium added to 84% saturation of the alginate. The Young's modulus and tensile stress at break increased in similar trends for gelling times up to 60 min followed by a slight decrease when the gelling time was further prolonged (Fig. 6A and B). Only minor differences were found in the nominal strain at break (Fig. 6C). Fig. 6D–F shows foams prepared from $CaCO_3$ with different specific surface areas, a constant calcium saturation of 84% and 60 min gelling time. Increased specific surface areas of $CaCO_3$ resulted in increasing Young's modulus

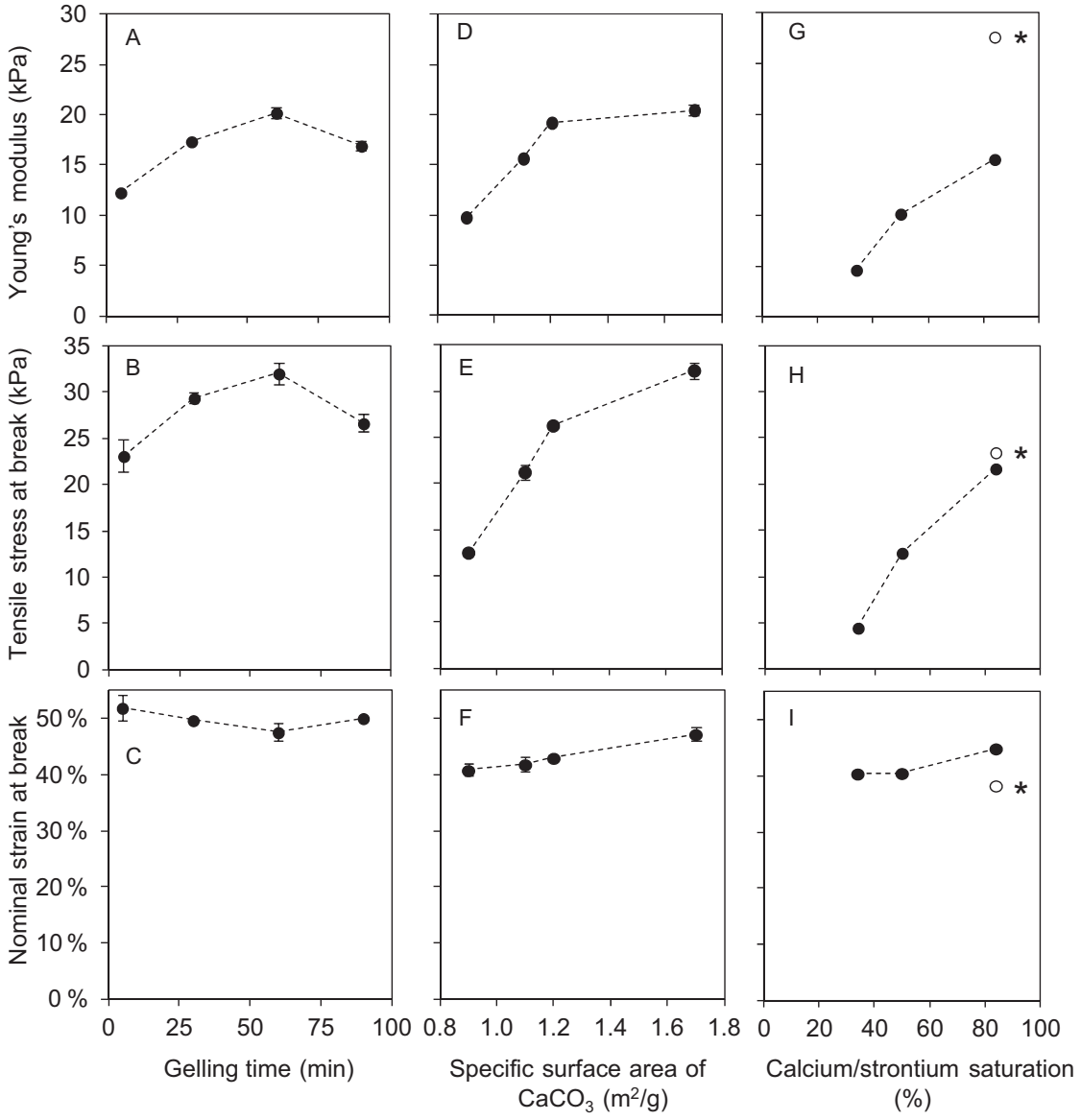

Fig. 6. The influence on mechanical properties Young's modulus, tensile stress at break and nominal strain at break of dried foams rehydrated in Hanks' solution as a function of gelling time before drying (A–C; $n = 6$), $CaCO_3$ particle surface area (D–F; $n = 10$) and calcium saturation (G–I; $n = 10$). Unless varied, the parameters were kept constant at 60 min gelling time, $CaCO_3$ specific surface area of 1.2 m^2/g and 84% calcium saturation. Dotted straight lines are added as guides to the eye. Error bars depict SE when exceeding the symbols. Significance is considered between foams where the alginate is saturated with 84% calcium or 84% strontium, $^*p < 0.05$. Symbols: (●) $CaCO_3$, (○) $SrCO_3$.

(Fig. 6D), increasing tensile stress at break (Fig. 6E) and to some extent increased stretch-ability was also seen (Fig. 6F). The foams shown in Fig. 6G–I have the alginate saturated with different saturations of calcium or 84% strontium. The prepared wet foams were gelled 60 min before drying and the $CaCO_3$ had a specific surface area of 1.2 m^2/g. With increasing calcium saturation, the hydrated foams exhibited an essentially linear increase in Young's modulus (Fig. 6G) and tensile stress at break (Fig. 6H), whereas the nominal strain a break showed only a slight increase for the highest calcium saturation (Fig. 6I). In comparison, foams prepared from $SrCO_3$ particles showed a significantly higher Young's modulus (Fig. 6G), similar tensile stress at break (Fig. 6H) and lower strain at break (Fig. 6I) compared to foams prepared with the same amount of $CaCO_3$.

As the gelling kinetic reflects the dissolution rate of $CaCO_3$ particles and the subsequent interaction between alginate and Ca^{2+} ions, an effect on mechanical properties by restricting the reaction time before drying can be expected (Fig. 6A–C). These differences are, however, likely also influenced by the drying conditions. As the release of Ca^{2+} is accelerated at increasing temperature (Kuo & Ma, 2001b), the gelling reaction in the foam will persist as long as sufficient amount of water is present or until complete cross-linking is achieved. In contrast, at higher temperatures water will be removed more rapidly through evaporation which again may hinder the completion of the gelling reaction. The slight reduction in elastic modulus and tensile stress at break seen for the foam allowed to gel for 90 min before drying (Fig. 6A and B), is likely related to a pore size that is less optimal for high mechanical properties due to increased coalescence (Fig. 4). The increased Young's modulus and tensile stress at break shown here by increasing specific surface areas of particles (Fig. 6D–F) is most likely due to a reduction in pore size and interconnectivity (Figs. 3 and 4A) as the foams contain a different and more dense distribution of pore walls. However, the gelling time was not adjusted to ensure complete dissolution of $CaCO_3$ and release of Ca^{2+} for each particle type before the wet foam was dried. Data by Moe et al. (1995) showed that although the gelling kinetics was influenced by the particle size of $CaCO_3$ used, the final elastic moduli of completely gelled hydrogels were similar. The increase in Young's modulus achieved by use of $SrCO_3$ compared to $CaCO_3$ at same concentration can be explained by the higher affinity of G-rich alginates for strontium (Mørch, Donati, Strand & Skjåk-Bræk, 2006; Smidsrød & Skjåk-Bræk, 1990). Although more elastic, the foams gelled with Sr^{2+} showed somewhat higher tensile stress at break and reduced strain at break, which can most likely be attributed to the influence of lower pore size.

Kuo and Ma (2001b) and Martinsen, Skjåk-Bræk, & Smidsrød (1989) showed a similar relationship between calcium content, modulus and strength when compressing hydrogels as seen here when rehydrated foams were stretched (Fig. 6G and H). These data together with the current results demonstrate the importance of gelling ion and gelling ion concentration selection on resultant alginate hydrogel mechanical properties. These findings are also supported by other reports in the literature (Banerjee et al., 2009; Huebsch et al., 2010; Place et al., 2011).

The internal gelling technique used to prepare alginate foams can result in an almost homogeneous distribution of alginate and calcium (Draget et al., 1991; Kuo & Ma, 2001b). However, the method described here will have a range of suitable $CaCO_3$/$SrCO_3$ particle sizes. Foam preparation with particles having too large specific surface areas may, for example, not be useful as the newly aerated wet foam may solidify too fast after addition of GDL, and it will not be enough time for molding. On the other hand, large particles with too small specific surface areas may sediment before dissolution and Ca^{2+}/Sr^{2+} binding to the alginate, resulting in inhomogeneity of the foam (Draget et al., 1991). This latter effect will also depend on the viscosity of the wet foam and may be compensated by increasing the alginate concentration, increasing the alginate molecular weight or by adding an additional viscosifier such as hyaluronate or xanthan (Draget et al., 1991). Improved gel homogeneity is also obtained (as done in the present work) by sonicating the $CaCO_3$ particles before use to reduce agglomeration and thereby increasing the rate of gelation (Draget et al., 1991; Moe et al., 1995). A blend of $CaCO_3$ particles of different size may also be used to optimize the properties of the foam. The gelling time may be considered as a processing parameter for preparation of the foam and it should be noticed that the completion of the gelling reaction also depend on the type of carbonate particles.

The dry alginate foams can be sterilized by standard sterilization techniques such as gamma (γ)-irradiation or treatment by ethylene oxide. Sterilization by γ-irradiation will degrade the alginate in the foams in a dose dependant manner and the mechanical properties of the foam will be reduced accordingly (Andersen, Melvik, et al., 2012; Andersen, Strand, et al., 2012b).

4. Conclusions

Herein we have described how the gelation rate of alginate in aerated foams can be utilized to tailor a variety of different physical foam characteristics. Internal gelation with different types and concentrations of $CaCO_3$/$SrCO_3$ resulted in foams with a range of average pore size, liquid absorbency and mechanical properties. The gelation rate was related to the specific surface area of $CaCO_3$/$SrCO_3$ particles and increased surface areas increased the rate of released gelling ions and hence the gelling of the alginate molecules. Increased gelation rate controlled by the surface area of the carbonate salts resulted in decreased pore size, increased fluid retention and higher absorbency capacity and mechanical integrity. Similar trends were achieved when the gelation rate was controlled by the concentration of gel forming ions.

Based on the relations in foam characteristics described here, the optimization of properties such as the pore size of a foam, can be controlled by the gelling time, concentration of gelling ions and/or source of gelling ions. In addition to the previously shown importance of operational and macromolecular parameters, the presented method for preparation of aerated and air dried alginate foams demonstrate a high flexibility in tuning physical characteristics of foams.

Appendix A. Supplementary data

Supplementary data associated with this article can be found, in the online version, at http://dx.doi.org/10.1016/j.carbpol.2013.08.036.

References

Al-Shamkhani, A., & Duncan, R. (1995). Radioiodination of alginate via covalently-bound tyrosinamide allows monitoring of its fate in vivo. *Journal of Bioactive and Compatible Polymers*, *10*, 4–13.

Alsberg, E., Kong, H. J., Hirano, Y., Smith, M. K., Albeiruti, A., & Mooney, D. J. (2003). Regulating bone formation via controlled scaffold degradation. *Journal of Dental Research*, *82*(11), 903–908.

Andersen, T., Melvik, J. E., Gåserød, O., Alsberg, E., & Christensen, B. E. (2012). Ionically gelled alginate foams: Physical properties controlled by operational and macromolecular parameters. *Biomacromolecules*, *13*(11), 3703–3710.

Andersen, T., Strand, B. L., Formo, K., Alsberg, E., & Christensen, B. E. (2012). Alginates as biomaterials in tissue engineering. In A. P. Rauter (Ed.), *Carbohydrate chemistry: Chemical and biological approaches – Glycosciences for human health and disease* (37) (pp. 227–258). London: Royal Society of Chemistry.

ASTM International. (2010). *ASTM D638-10 standard test method for tensile properties of plastics*. West Conshohocken: ASTM International.

Augst, A. D., Kong, H. J., & Mooney, D. J. (2006). Alginate hydrogels as biomaterials. *Macromolecular Bioscience*, *6*(8), 623–633.

Banerjee, A., Arha, M., Choudhary, S., Ashton, R. S., Bhatia, S. R., Schaffer, D. V., et al. (2009). The influence of hydrogel modulus on the proliferation and differentiation of encapsulated neural stem cells. *Biomaterials*, *30*(27), 4695–4699.

Barbetta, A., Barigelli, E., & Dentini, M. (2009). Porous alginate hydrogels: Synthetic methods for tailoring the porous texture. *Biomacromolecules*, *10*(8), 2328–2337.

Bencherif, S. A., Sands, R. W., Bhatta, D., Arany, P., Verbeke, C. S., Edwards, D. A., et al. (2012). Injectable preformed scaffolds with shape-memory properties. *Proceedings of the National Academy of Sciences of the United States of America*, *109*(48), 19590–19595.

Boateng, J. S., Matthews, K. H., Stevens, H. N. E., & Eccleston, G. M. (2008). Wound healing dressings and drug delivery systems: A review. *Journal of Pharmaceutical Sciences*, *97*(8), 2892–2923.

Boontheekul, T., Kong, H. J., & Mooney, D. J. (2005). Controlling alginate gel degradation utilizing partial oxidation and bimodal molecular weight distribution. *Biomaterials*, *26*(15), 2455–2465.

BSI British Standards. (2002). *BS EN 13726-1:2002 test methods for primary wound dressings – Part 1. Aspects of absorbency*. London: British Standards Institution.

Donati, I., Holtan, S., Mørch, Y. A., Borgogna, M., Dentini, M., & Skjåk-Bræk, G. (2005). New hypothesis on the role of alternating sequences in calcium-alginate gels. *Biomacromolecules*, *6*(2), 1031–1040.

Draget, K. I., Smidsrød, O., & Skjåk-Bræk, G. (2005). Alginates from algae. In S. K. Rhee, & A. SteinBüchel (Eds.), *Polysaccharides and polyamides in the food industry. Properties, production, and patents* (pp. 1–30). Weinheim: Wiley-VCH.

Draget, K. I., Østgaard, K., & Smidsrød, O. (1991). Homogeneous alginate gels: A technical approach. *Carbohydrate Polymers*, *14*, 159–178.

Drury, J. L., & Mooney, D. J. (2003). Hydrogels for tissue engineering: Scaffold design variables and applications. *Biomaterials*, *24*(24), 4337–4351.

Dvir-Ginzberg, M., Elkayam, T., & Cohen, S. (2008). Induced differentiation and maturation of newborn liver cells into functional hepatic tissue in macroporous alginate scaffolds. *FASEB Journal*, *22*(5), 1440–1449.

Fang, Y., Al-Assaf, S., Phillips, G. O., Nishinari, K., Funami, T., Williams, P. A., et al. (2007). Multiple steps and critical behaviors of the binding of calcium to alginate. *Journal of Physical Chemistry B*, *111*(10), 2456–2462.

Freeman, I., Kedem, A., & Cohen, S. (2008). The effect of sulfation of alginate hydrogels on the specific binding and controlled release of heparin-binding proteins. *Biomaterials*, *29*(22), 3260–3268.

Funami, T., Fang, Y., Noda, S., Ishihara, S., Nakauma, M., Draget, K. I., et al. (2009). Rheological properties of sodium alginate in an aqueous system during gelation in relation to supermolecular structures and Ca^{2+} binding. *Food Hydrocolloids*, *23*, 1746–1755.

Grayson, W. L., Martens, T. P., Eng, G. M., Radisic, M., & Vunjak-Novakovic, G. (2009). Biomimetic approach to tissue engineering. *Seminars in Cell and Developmental Biology*, *20*(6), 665–673.

Haug, A., & Smidsrød, O. (1970). Selectivity of some anionic polymers for divalent mateal ions. *Acta Chemica Scandinavica*, *24*, 854–873.

Hegge, A. B., Andersen, T., Melvik, J. E., Bruzell, E., Kristensen, S., & Tønnesen, H. H. (2011). Formulation and bacterial phototoxicity of curcumin loaded alginate foams for wound treatment applications: Studies on curcumin and curcuminoides XLII. *Journal of Pharmaceutical Sciences*, *100*(1), 174–185.

Hegge, A. B., Andersen, T., Melvik, J. E., Kristensen, S., & Tønnesen, H. H. (2010). Evaluation of novel alginate foams as drug delivery systems in antimicrobial photodynamic therapy (aPDT) of infected wounds—An in vitro study: Studies on curcumin and curcuminoides XL. *Journal of Pharmaceutical Sciences*, *99*(8), 3499–3513.

Henderson, T. M. A., Ladewig, K., Haylock, D. N., McLean, K. M., & O'Connor, A. J. (2013). Cryogels for biomedical applications. *Journal of Materials Chemistry B*, *1*, 2682–2695.

Holte, O., Tønnesen, H. H., & Karlsen, J. (2006). Measurement of diffusion through calcium alginate gel matrices. *Pharmazie*, *61*(1), 30–34.

Huebsch, N., Arany, P. R., Mao, A. S., Shvartsman, D., Ali, O. A., Bencherif, S. A., et al. (2010). Harnessing traction-mediated manipulation of the cell/matrix interface to control stem-cell fate. *Nature Materials*, *9*(6), 518–526.

Hwang, C. M., Sant, S., Masaeli, M., Kachouie, N. N., Zamanian, B., Lee, S. H., et al. (2010). Fabrication of three-dimensional porous cell-laden hydrogel for tissue engineering. *Biofabrication*, *2*, 1–12, 035003

Jain, J. P., Ayen, W. Y., Domb, A. J., & Kumar, N. (2011). Biodegradable polymers in drug delivery. In A. J. Domb, N. Kumar, & A. Ezra (Eds.), *Biodegradable polymers in clinical use and clinical development* (pp. 3–58). New York: John Wiley & Sons, Inc.

Kong, H. J., Alsberg, E., Kaigler, D., Lee, K. Y., & Mooney, D. J. (2004). Controlling degradation of hydrogels via the size of cross-linked junctions. *Advanced Materials*, *16*(21), 1917–1921.

Kong, H. J., Smith, M. K., & Mooney, D. J. (2003). Designing alginate hydrogels to maintain viability of immobilized cells. *Biomaterials*, *24*(22), 4023–4029.

Kristiansen, K. A., Tomren, H. B., & Christensen, B. E. (2011). Periodate oxidized alginates: Depolymerization kinetics. *Carbohydrate Polymers*, *86*(4), 1595–1601.

Kuo, C. K., & Ma, P. X. (2001a). Controlling diffusion of solutes through ionically crosslinked alginate hydrogels designed for tissue engineering. In *Mat Res Soc Symp Proc, vol. 662* Materials Research Society.

Kuo, C. K., & Ma, P. X. (2001b). Ionically crosslinked alginate hydrogels as scaffolds for tissue engineering. Part 1. Structure, gelation rate and mechanical properties. *Biomaterials*, *22*(6), 511–521.

Lai, H. L., Abu'Khalil, A., & Craig, D. Q. M. (2003). The preparation and characterisation of drug-loaded alginate and chitosan sponges. *International Journal of Pharmaceutics*, *251*(1/2), 175–181.

Lee, K. Y., & Mooney, D. J. (2012). Alginate: Properties and biomedical applications. *Progress in Polymer Science*, *37*(1), 106–126.

Leone, G., Barbucci, R., Borzacchiello, A., Ambrosio, L., Netti, P. A., & Migliaresi, C. (2004). Preparation and physico-chemical characterisation of microporous polysaccharidic hydrogels. *Journal of Materials Science – Materials in Medicine*, *15*(4), 463–467.

Li, Z. S., Ramay, H. R., Hauch, K. D., Xiao, D. M., & Zhang, M. Q. (2005). Chitosan-alginate hybrid scaffolds for bone tissue engineering. *Biomaterials*, *26*(18), 3919–3928.

Martinsen, A., Skjåk-Bræk, G., & Smidsrød, O. (1989). Alginate as immobilization material. I. Correlation between chemical and physical properties of alginate gel beads. *Biotechnology and Bioengineering*, *33*(1), 79–89.

Miralles, G., Baudoin, R., Dumas, D., Baptiste, D., Hubert, P., Stoltz, J. F., et al. (2001). Sodium alginate sponges with or without sodium hyaluronate: In vitro engineering of cartilage. *Journal of Biomedical Materials Research*, *57*(2), 268–278.

Moe, S. T., Draget, K. I., Skjåk-Bræk, G., & Smidsrød, O. (1995). Alginate. In A. Stephen (Ed.), *Food polysaccharides and their applications* (9) (pp. 245–286). New York: Marcel Dekker.

Mørch, Y. A., Donati, I., Strand, B. L., & Skjåk-Bræk, G. (2006). Effect of Ca^{2+}, Ba^{2+}, and Sr^{2+} on alginate microbeads. *Biomacromolecules*, *7*(5), 1471–1480.

Place, E. S., Rojo, L., Gentleman, E., Sardinha, J. P., & Stevens, M. (2011). Strontium- and zinc-alginate hydrogels for bone tissue engineering. *Tissue Engineering Part A*, *17*(21/22), 2713–2722.

Re'em, T., Tsur-Gang, O., & Cohen, S. (2010). The effect of immobilized RGD peptide in macroporous alginate scaffolds on TGF beta 1-induced chondrogenesis of human mesenchymal stem cells. *Biomaterials*, *31*(26), 6746–6755.

Rowley, J. A., Madlambayan, G., & Mooney, D. J. (1999). Alginate hydrogels as synthetic extracellular matrix materials. *Biomaterials*, *20*(1), 45–53.

Sapir, Y., Kryukov, O., & Cohen, S. (2011). Integration of multiple cell-matrix interactions into alginate scaffolds for promoting cardiac tissue regeneration. *Biomaterials*, *32*(7), 1838–1847.

Shapiro, L., & Cohen, S. (1997). Novel alginate sponges for cell culture and transplantation. *Biomaterials*, *18*(8), 583–590.

Simmons, C. A., Alsberg, E., Hsiong, S., Kim, W. J., & Mooney, D. J. (2004). Dual growth factor delivery and controlled scaffold degradation enhance in vivo bone formation by transplanted bone marrow stromal cells. *Bone*, *35*(2), 562–569.

Smidsrød, O., & Skjåk-Bræk, G. (1990). Alginate as immobilization matrix for cells. *Trends in Biotechnology*, *8*(3), 71–78.

Thornton, A. J., Alsberg, E., Albertelli, M., & Mooney, D. J. (2004). Shape-defining scaffolds for minimally invasive tissue engineering. *Transplantation*, *77*(12), 1798–1803.

Tønnesen, H. H., & Karlsen, J. (2002). Alginate in drug delivery systems. *Drug Development and Industrial Pharmacy*, *28*(6), 621–630.

Wee, S., & Gombotz, W. R. (1998). Protein release from alginate matrices. *Advanced Drug Delivery Reviews*, *31*(3), 267–285.

Zmora, S., Glicklis, R., & Cohen, S. (2002). Tailoring the pore architecture in 3-D alginate scaffolds by controlling the freezing regime during fabrication. *Biomaterials*, *23*(20), 4087–4094.